POLITECNICO
MILANO 1863

Space Propulsion Project

Study of MEMs propulsion systems for CubeSat applications

Matteo Maria Basci, Emanuele Bianco, Filippo Chini, Antonio De Gennaro, Federico Ferrara, Chiara Alessia Guffanti, Mantas Kazenas, Luca Matteotti, Riccardo Mazzitti

April, 2025

Contents

List of Figures

Abstract

The miniaturization of propulsion systems is a critical step towards the advancing of nano and micro satellite capabilities, in particular for CubeSats. The following paper has the objective to build up a solid background on MEMs and to develop a comparative design among the different propulsion solutions, including cold gas, bipropellant, solid and vaporizing thrusters. Through the arrangement of some fundamental parameters referred to a $3U$ CubeSat and merging the data with currently available literature about micro-propulsion, a nominal design for each of the aforementioned systems has been provided, with the addition of a sizing of the said model. Considering that every system is characterized by its own uncertainties, the study will focus on the nozzle construction accuracy, taking account of the respective uncertainties and their propagation on the thrust profile by performing a Monte Carlo analysis. The results highlight different possibilities of trade-offs between complexity, performances and power consumption, providing a framework for selecting optimal MEMS propulsion architectures.

1 Introduction

The recent development of micro and nano technologies has allowed a rapid advancement in CubeSat and PocketSat technology and more generally, in miniaturized propulsion systems. This kind of systems have to maintain a relatively high performance despite all the issues of the miniaturization process such as mass, volume and power limitations.
Micro-Electro-Mechanical Systems (MEMs)-based micronozzles are one of the components that have become a crucial part of micro propulsion, in view of the fact that they provide scalability and accuracy that traditional macroscale thrusters cannot match.
MEMs micronozzles can work with a wide range of different propulsion systems, such as cold gas, bipropellant, monopropellant, and vapor thrusters, but several of them are still in the experimental stage.
Despite their simplicity, cold gas thrusters are characterized by a low efficiency, as a result of viscous losses at low Reynolds numbers. Even though bipropellant and monopropellant systems have greater specific impulses, they still have to deal with the challenge of shrinking the dimensions of the catalyst and the combustion chambers. Resistojets and other vapor-based thrusters use electrical heating to improve performance, but they also need a precise nozzle design and thermal control to lower the rarefaction effects in microscale flows.
MEMs optimization is generally challenging due to microscale phenomena; in fact real gas dynamics, boundary layer dominance and manufacturing tolerances pose a big theoretical and engineering problem. To solve these problems, recent researches focused on material innovations and geometric modifications such as expansion ratios and throat profiles, however, more studies are still needed to build a solid and complete background knowledge about this topic [30].

2 MEMS in Modern Engineering: A Review of Technological Progress and Research Gaps

2.1 Microscale Mechanics with Macroscale Potential

MEMs are miniaturized systems integrating mechanical elements, sensors, actuators and electronics on a common substrate using micro-fabrication techniques. Operating at microscales, these systems enable complex functionalities in compact and low power devices. The main advantages are related to their little dimensions and high functional density, making them perfect for nano satellite applications. However, they present multiple challenges related to the miniaturization such as manufacturing complexity, packaging and integration, as micro structures are really sensitive to contamination, mechanical stresses and scaling effects. Micro fluid dynamics introduces different critical challenges related to forces, such as surface tension and viscous drag prevailing over inertia, thus affecting the overall performance. Despite these issues, the advantages are so relevant that a large number of modern studies are concentrated in developing and improving MEMs technology. [30]

Cold Gas Micro-Thrusters (CGT) It is one of the simplest types of micro-propulsion system and it relies on the expansion of a compressed inert gas accelerated through a nozzle to produce thrust with no chemical reactions. The construction simplicity makes cold gas thrusters reliable and easy to integrate in nano satellites. Generally the system is composed by a tank, containing the compressed or liquefied gas, a micronozzle and an architecture to modulate the gas release. Due to the fact that combustion processes are not present, the gas exits the nozzle at ambient temperature, meaning a lower exhaust velocity and lower specific impulse compared to chemical thrusters. The main advantages are the precision and the repeatability of the pulse with a great on-off control and throttleability. The levels of thrust provided by cold gas micro-thrusters span from few μN to several mN with a low power consumption. Other than the problem related to miniaturization, the main challenges are maximizing the thrust-to-mass ratio, in particular when tank mass dominates, and optimizing the propellant storage, especially for high-density liquefied gasses [4].

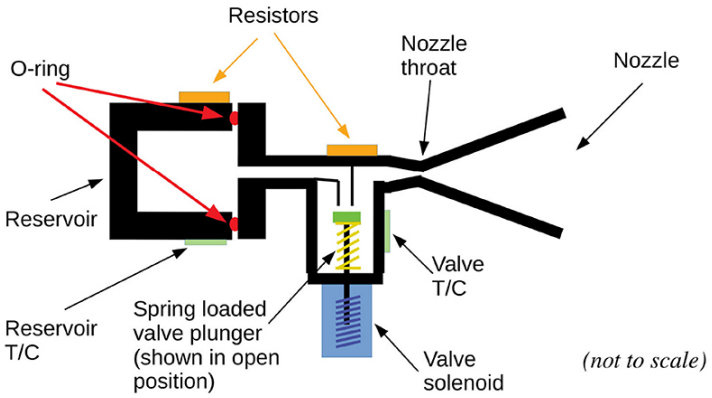

Figure 1: CGT system schematic

Bipropellant Micro-Thrusters It is a miniaturized propulsion system that relies on two separate chemical components, a fuel and an oxidizer, that react spontaneously (in hypergolic systems) or through ignition generating high temperature and high pressure gasses. The gases are accelerated through a nozzle in order to produce thrust. The system can be schematized in two tanks, one for the fuel and one for the oxidizer, a combustion chamber, a converging-diverging nozzle and micro-channels for fluid transport. The most important design challenges are the fuel management, in particular the oxidizer to fuel ratio, the thermal management of the combustion chamber and the nozzle optimization. Compared to other propulsion systems, the main advantages of this technology are a high specific impulse, due to energetic combustion, fine thrust control, flow rate and burn duration can be controlled, and a great thrust output with respect to system size. On the other hand, the most remarkable disadvantage is the high system complexity that leads to an expensive propulsion system. The Bipropellant micro-thrusters also present all the problematic related to miniaturization, such as production and micro-fluid dynamics management. The most advanced bipropellant micro-thrusters can deliver thrust from hundred of μN to several mN with a power consumption in the range of 1 to 5 W. The trade-off between performance and complexity makes bipropellant micro-thruster well suited for those missions that require precise maneuvering [30].

Solid Propellant Micro-Thruster (SPM) This one is a type of MEMs based on the controlled ignition and combustion of a solid propellant stored within micromachined holes on a silicon or glass substrate. The main elements composing an SPM are the propellant chamber, ignition system and micro-nozzle. The solid propellant, typically a stable energetic material, does not require a feed system, making the low complexity, low mass platform and high shelf life its biggest advantages. The activation of an igniter, often based on resistive heating or thin-film plasma ignition, triggers the combustion, generating gases at high temperature that are

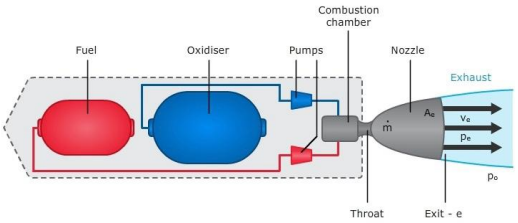

Figure 2: Bipropellant Micro-Thruster schematic

accelerated and expelled by the micro-nozzle in order to generate thrust. The main difficulties related to this kind of thrusters are the following:

- igniter integration and reliability, since the burn is often non-repeatable it's fundamental to have a high level of reliability;
- thermal isolation, in order to avoid undesired ignition of adjacent thruster (SPM are usually disposed in arrays);
- combustion gas expansion and nozzle flow, the biggest problems arise from micro-fluid dynamics;
- production and propellant loading related to the microscale of SPMs.

The biggest limit of those systems is that they are not throttleable or restartable, therefore each unit can provide only a single impulse. For this reason solid propellant microthruster are often fabricated in wafer arrays. Modern SPMs can deliver a thrust from tens of μN up to few mN with low power consumption in the order of hundreds of mW to few W during ignition making them suitable for spacecrafts with limited energy budgets [19].

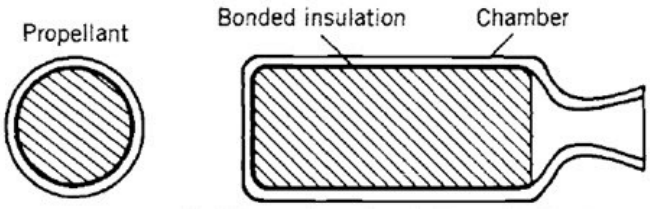

Figure 3: SPM system schematic

Vaporizing Liquid Micro-thrusters (VLM) This variety of MEMs propulsion system consists of an inlet channel through which the propellant is fed, a heating chamber in which the propellant is vaporized due to the presence of some resistive heaters and a nozzle that accelerates the gases. The most significant aspects of these propulsion systems, on which the analyses have been focused, are the design of the chamber, the boiling process and the numerical analysis of flow in micro nozzles. Materials and configuration of the heating elements are of particular attention, since they are the key features for what concerns the performance improvement due to the low efficiency energy conversion.
In nano satellites applications, water is used as a propellant since it can be stored as liquid and it is safe to handle. The primary drawback is a great power consumption due to the high enthalpy of vaporization, yet it can still meet the expected requirements for small satellites. Despite this disadvantage, water provides the best change in velocity per volume of propellant and also the best specific impulse, with respect to other suitable substances.
There are two different designs that derive from the different manufacturing processes chosen. One configuration is with the nozzle perpendicular (out-of-plane) to the plane of the wafer. This simplifies manufacturing, but it

reduces the freedom of design and degrades performance. The other possibility is to create out-of-plane nozzles with more complex shapes. State-of-the-art devices can deliver thrust in the range of around 1 µN to around 7 mN while consuming from 1 to 10 W, which could be high depending on the type of mission. [30]

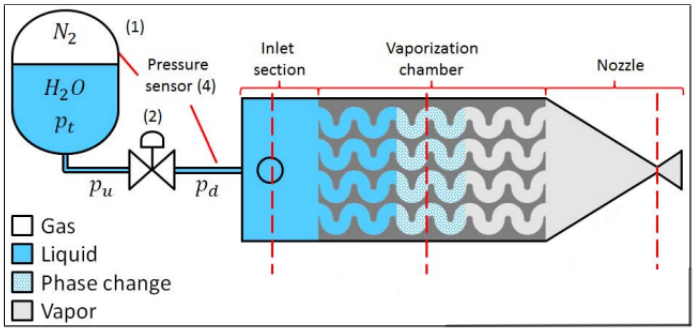

Figure 4: VLM system schematic showing the presence of a tank, a valve and the vaporization chamber

2.2 Efficiency of Micro-nozzles

When talking about the efficiency of a nozzle that has microscopic sizes there are several variables that need to be taken into account: [32] [18]

Inlet and Exit Pressure The influence of inlet pressure on the specific impulse diminishes with the increasing of pressure and, at around 50 kPa, there is no reason to modify the pressure in order to gain specific impulse. At that point, a further rise in the inlet pressure would result in additional structural stress only, without noteworthy results. Generally the lower the exit pressure, the better for micro-nozzles, as they typically operate at the lower end of inlet pressure and this means that there are reduced chances of under expansion. So, operating in near vacuum is the perfect condition for micro nozzles, as it allows the propellant to expand more completely increasing I_s and thrust.

Nozzle Thermal Effects Tests have shown that the Reynolds number in the throat and the thrust decrease with the temperature, but specific impulse increases nearly linearly with the temperature. Moreover, the temperature has more effect on specific impulse than the thrust force; when T grows from 300 K to 400 K, I_s increases by 14.7%, while the thrust only decreases by around 1.4% .

Nozzle Geometry Micro nozzles with a typical throat diameter of 10^{-4}–$10^{-5}m$ are subject to rarefied effects resulting from their reduced size, making the thrust, specific impulse and efficiency, highly dependent on their geometric feature. The decrease in throat width leads to a decrease in Reynolds number and then a decrease in thrust force.

Expansion Ratio At a chamber pressure of 1 kPa both thrust and I_s decrease as the expansion ratio ε increases. However, at higher chamber pressures between 10 kPa and 50 kPa, thrust and I_s show a positive correlation with the expansion ratio, increasing steadily before leveling off when $\varepsilon \geq 8.9$, which is a trend featured in macroscopic nozzles. Micro nozzles performances lie in the compromise between flow expansion, which can be enhanced by a larger expansion ratio, and boundary layer losses near the nozzle walls. Indeed, while greater flow expansion improves performance, increased wall friction has the opposite effect.

Channel Configuration The shape of the channel has a great impact on flow characteristics, while it has little impact on nozzle performance. However, the angle of the section of the divergent affects the flow separation and the viscous losses. The process of optimizing the divergence angle is crucial for minimizing these losses and improving overall nozzle efficiency.

3 Numerical and Analytical Modeling of Micro-Electro-Mechanical Systems

In the process of sizing different propulsion unit for a 3U CubeSat, the following geometrical and performance constraints have been considered:

- Dimensions: 10 cm x 10 cm x 30 cm. [1]
- Dry mass: 2 kg. [1]
- Nominal thrust: 5 mN.
- Total Δv provided: 0.5 m/s

The values of nominal thrust and Δv have been chosen in order to mirror existing mission of 3U-CubeSats, that are becoming the main focus of future space missions. In order to improve their capabilities, the micro propulsion systems are greatly evolving and are an interesting topic to focus in academic studies, such as this one. The main modeling goal of this study is the development of comparative designs among the four different propulsion solutions that have been briefly introduced in the previous chapter.
For each solution, a nominal design has been modeled and also, a volume compatible with the satellite requirements has been computed. Moreover, the power required for each unit to operate has been considered and it must comply with the power requirements of a standard CubeSat. Furthermore, single or multiple engines configurations have been investigated.
As a general assumption, the presence of an additional volume between the valve and the injection plate was taken into account. It is called plenum and is used to maintain the flow regular and to reach an almost total pressure condition before injection in the chamber.
Additionally, the nominal pressures in every chamber have been selected from reference literature and moreover, the entire modeling process is guided by taking into account previous studies as reference.

3.1 Vapor expansion thruster

The study of the vapor expansion system was founded on a water-based (ρ_{water} = 997.05 kg/m^3) Vaporizing Liquid Micro-thruster, where the chamber and the micronozzle have been fabricated utilizing anisotropic wet etching of silicon. The heating of the propellant is provided by means of platinum resistive micro-heaters. The chosen configuration is similar to the one displayed in fig. 5.

3.1.1 Model Assumptions

The following hypothesis have been considered during the computation of the parameters of this particular propulsion system and for the sizing of its elements:

- The propellant used is water, since it can accelerate the spacecraft to higher velocities using the same volume of propellant with respect to other candidates. Moreover, water ensures safe operational environment, it is environmentally friendly and cheap, it has high density and it is stable enough to be stored in a weakly pressurized light tank.

[1] Typical values for CubeSat applications

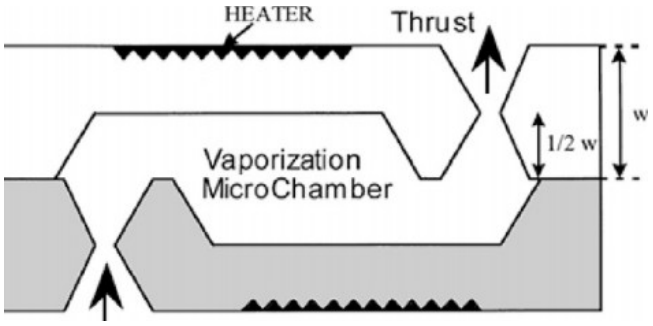

Figure 5: VLM model with out-of-plane thrust

- The effects of friction inside the small volumes of the system have been neglected.
- The water vapor generated in the vaporizing chamber has been considered as a calorically perfect gas.
- The power generated by the resistive heaters is not subjected to dispersion; it goes directly into heating the flowing liquid in the vaporizing chamber.
- The temperature at the inlet is at standard conditions (25° C) while there are no constraints for the inlet pressure.
- The flow from the exit convergent nozzle is isentropic, while in the vaporizing chamber is assumed adiabatic since the volume is limited and as a consequence, the temperature does not vary significantly.
- For what concerns the pressurization system of the propellant, the presence of a valve and a pressure regulator have been taken into account.
- The nozzle section angles (convergent and divergent) are assumed to fall within the typical range observed in comparable cases.

3.1.2 Performances Analysis and Chamber Sizing

The aim of this section is to completely size the VLM propulsion unit, which is composed of an inlet, a vaporizing chamber and a convergent-divergent conical nozzle.
The characterization process started with the choice of three initial parameters: a total pressure value P_c in the vaporizing chamber of 300 kPa, which is in the range of typical pressure chamber values found in past developed VLM [29]; a chamber temperature T_c of 450 K , higher than the vaporization temperature of water to overheat the chamber and obtaining a full vaporization, and also to consider the maximum operating temperature of the construction material (Silicon: T_{max}= 523 K); an expansion ratio ε equal to 4.34 to achieve a nozzle efficiency in the range of existing VLMs, since:

$$\eta_{nozzle} = 1 - \left(\frac{P_e}{P_c}\right)^{\frac{\gamma-1}{\gamma}} = 0.5811 \tag{1}$$

where $\gamma = 1.33$ is the specific heat ratio of water vapor. This equation discloses the correlation between the nozzle efficiency, which is defined by how much kinetic energy the nozzle creates with respect to the maximum possible one, and the pressure ratio, which is,in turn, influenced by the geometry of the nozzle (expansion ratio ε) [21]. The selection of these parameters enables the computation of the values of velocity, pressure and temperature at the exit of the nozzle by using the isentropic relations of the nozzle expansion:

Exit temperature	Exite pressure	Exit velocity
T_e [K]	P_e [Pa]	v_e [m/s]
188.52	9000	986.6715

Table 1: Values at the exit of the nozzle

It's important to note that the resulting exit temperature is very low (−84.58 °C) and this could create ice in the nozzle, endangering the VLM. This could be prevented by adjusting the expansion ratio ε or the T_c and could be an interesting matter to discuss in another study.
Since a VLM system works by accelerating a hot vapor through a nozzle, one key aspect of the sizing is the power consumption of the micro-heaters located in the chamber. It is possible to compute the power consumption W by using equation 2.

$$W = \dot{m}\left[c_{p_{\text{wat}}}(T_v - T_i) + L_v + c_{p_{\text{vap}}}(T_c - T_v)\right] \tag{2}$$

Thermodynamic Properties		Temperature Values	
Water specific heat: $\boldsymbol{C_{p,wat}}$	4182 J/(kg K)	Inlet temperature: $\boldsymbol{T_i}$	25 °C
Vapor specific heat: $\boldsymbol{C_{p,vap}}$	2100 J/(kg K)	Chamber temperature: $\boldsymbol{T_c}$	176.9 °C
Latent heat of vaporization: $\boldsymbol{L_v}$	2163.4 kJ/kg	Water vaporization temperature: $\boldsymbol{T_v}$	133.4 °C

Table 2: Values for liquid water and water vapor

The water vaporization temperature T_v is a function of the P_c and can be obtained by exploiting the Antoine equation:

$$T_v = \frac{B}{A - \log_{10}(P_c)} + C \tag{3}$$

with: $A = 10.27$, $B = 1810.94$ and $C = 28.67$ [29].
To obtain the mass flow rate $\dot{m}$, and then the power W, it was necessary to solve the system equation 4, in which the other unknown in the system is the throat area A_t, composed of the equations of the thrust, considering the 2D-losses in the nozzle, and of the mass flow rate [1].

$$\begin{cases} T = \lambda \dot{m} v_e + P_e \varepsilon A_t \\ \dot{m} = \dfrac{\Gamma P_c A_t}{\sqrt{\dfrac{R}{M_{mol}} Tc}} \end{cases} \tag{4}$$

In this system of equations, $M_{mol} = 18\,\text{g/mol}$, $R = 8.314\,\text{J/molK}$ and $\Gamma(\gamma)$ is the *Vandenkerckhove* function, which depends on γ. The 2D-losses are represented with the correcting factor $\lambda = 0.9330$, which embodies a half-angle of the divergent part of the nozzle $\alpha = 30°$.

Mass flow rate	Throat area	Power consumption
$\dot{m}$ [mg/s]	A_t [mm^2]	P [W]
4.9562	0.0112	13.4220

Table 3: Nominal values computed

The values of $\dot{m}$ and A_t are in the range of usual measures for micro-thrusters, highlighting their microscopical nature, as can be seen by [29] [9]; on the other hand the value of the power consumption is too high for a

3U-CubeSat, since the usual range of power generation is 1 – 10 W [30], and this represents the major criticality in the use of VLM for small satellites.
Another important value to analyze in order to study the performance of this kind of micro-thrusters is the specific impulse, which is useful also for the sizing of the tanks, as seen in the next paragraph, that is computed by:

$$I_{sp} = \frac{T}{\dot{m} g_0} \tag{5}$$

The value computed, $I_{sp} = 102.84$ s, represents a good performance for the VLM computed, being in the same range of an advanced VLM prototype [5], shown in Figure 6.

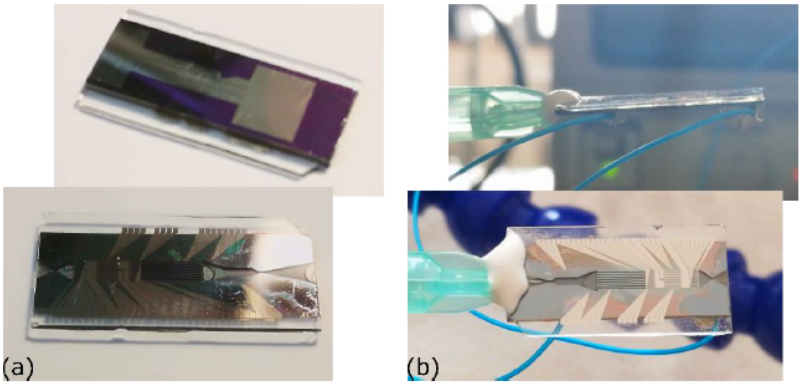

Figure 6: Prototype of VLM [5]

One of the initial assumption is the isothermic nature of the vaporization chamber, also stated in [31], which results in a very low Mach number in the chamber ($M_c = 0.1$), from which the combustion chamber area is obtained:

$$A_c = \frac{A_t}{M_c} \left[\frac{2}{k+1} \left(1 + \frac{k+1}{2} M_c^2 \right) \right]^{\frac{k+1}{2(k-1)}} \tag{6}$$

On the assumption that the heating chamber has a circular area, the computed diameter is $d_c = 0.2943$ mm; instead of a single chamber, prototypes in development prefer to use multiple micro-channels with smaller radius since the high heat transfer efficiency is increased thanks to the increased surface-to-volume ratio, as in the case described before [5]. The length of the heating chamber was chosen by looking at the same prototype [5], $L_c = 9$ mm, this high value is chosen in order to heat all the water up to vaporization temperature with a reduced electric power consumption for the heaters. From these values the volume of the chamber was finally computed: $V_c = A_c L_c = 0.6123\,\text{mm}^3$.
After having computed the exit, throat and chamber areas, to complete the sizing of the convergent-divergent nozzle the only values left are the lengths of both the divergent and convergent. Since the nozzle is assumed conical these values can be computed by choosing the half-angles $\alpha = 30°$ and $\beta = 30°$, which were chosen in order to study the 2D-losses in the nozzle:

$$L_{Div} = \frac{1}{2} \frac{d_e - d_t}{tan(\alpha)} \tag{7}$$

$$L_{Conv} = \frac{1}{2} \frac{d_c - d_t}{tan(\beta)} \tag{8}$$

The results are shown in table 4; the total length of the nozzle is very small compared to the one of the chamber, this is due multiple factors such as reducing viscous losses and simplicity in the micro-fabrication processes

L_{Div}	L_{Conv}	L_{Nozzle}
0.1120 mm	0.1515 mm	0.2635 mm

Table 4: Nozzle dimensions

[24]. The last section of the VLM to be computed is the area of the propellant injector before the heating chamber, to do so, since the water in this section is still in liquid phase, we exploit equation 9:

$$A_{inj} = \frac{\dot{m}}{c_D \sqrt{2\Delta P_{inj} \rho_{Prop}}} \tag{9}$$

where $c_D = 0.7$ is the assumed discharge coefficient, that depends on the geometry (conic form) of the injection inlet, and ΔP_{inj} represents the pressure drop in the orifice and was computed as $\Delta P_{inj} = 15\% P_c = 45$ kPa. The injection area obtained is $A_{inj} = 7.4110 \cdot 10^{-4}\ mm^2$, with a diameter of $d_{inj} = 31$ µm; a value this low makes necessary the use of an injection needle, for example a 33G needle as in the study shown in [10].

3.1.3 Propellant Tank Sizing

The proposed architecture of the pressurization system is similar to the one represented in fig. 7. The pressurant gas and the water are stored together in the same tank, while the pressure of the liquid is controlled by a pressure regulator. Helium gas has been selected as the pressurant gas that pushes the liquid water towards the injection needle. In light of these considerations, the pressurization system has been modeled as pressure regulated.
In order to compute the volume of the tank that is necessary to provide a pressure in the chamber of 300 kPa, a *pressure cascade method* has been adopted. In addition, a temperature of 298 K in the pressurization tank (T_{tank}) has been assumed.
Owing to the Tsiolkovsky equation, it was possible to evaluate the mass ratio MR that is necessary to compute the wet mass: $M_{wet} = M_{dry} \cdot MR$. Considering that the dry mass of the CubeSat is equal to 2 kg, the mass of propellant onboard is: $M_{prop} = M_{wet} - M_{dry}$. The previous steps were necessary in order to compute the volume of the propellant (from M_{prop}, knowing the liquid water density) since it is parameter needed to estimate the tank volume as follows: $V_{tank} = V_{gas} + V_{prop}$, where V_{gas} is the volume of helium present in the tank.
Before the computation of V_{gas}, it is essential to evaluate the mass of the pressurant gas with the equation 10.

$$M_{gas} = \frac{P_{tank} \cdot V_{prop}}{R_{gas} \cdot T_{tank}} \cdot \frac{\gamma}{1 - \frac{P_{gas,f}}{P_{gas,i}}} \tag{10}$$

where, for helium, $R = 2077.3$ J/kgK and $\gamma = 1.67$; the initial pressure of the gas $P_{gas,i}$ is assumed to be 10 times larger than the pressure in the tank P_{tank} (as common practice); the final pressure of the gas $P_{gas,f}$ is the same as P_{tank}.
Using the pressure cascade method, which considers all the pressure losses in the feeding system, P_{tank} has been obtained as shown in equation 11.

$$P_{tank} = 1.15 \cdot P_{chamber} + \Delta P_{dyn} + \Delta P_{feed} \tag{11}$$

where the 1.15 factor embeds the injection losses (assumed equal to 15% of the chamber pressure); ΔP_{feed} are the feeding lines losses (a typical value of 35 kPa has been chosen); ΔP_{dyn} are the dynamic losses. As final step, using the Ideal Gas Law and considering that $T_{gas} = T_{tank}$, the initial volume of the pressurant gas has been obtained.

As expected for a miniaturized propulsion system, the volumes indicated in table 5 are small. These outcomes translate in a space saving that is of fundamental importance for nanosatellites.

Volume of propellant	Volume of gas	Volume of the tank
V_{prop} [cm^3]	V_{gas} [cm^3]	V_{tank} [cm^3]
0.9860	0.1830	1.1690

Table 5: Results of the sizing of the pressurization tank

In the light of the results of the complete sizing process for the VLM, it has been verified that a single-engine configuration is able to fulfill the specified values of thrust and furthermore, the resultant volume of the vaporizing chamber is compatible with the dimension of the overall unit for a 3U CubeSat application.

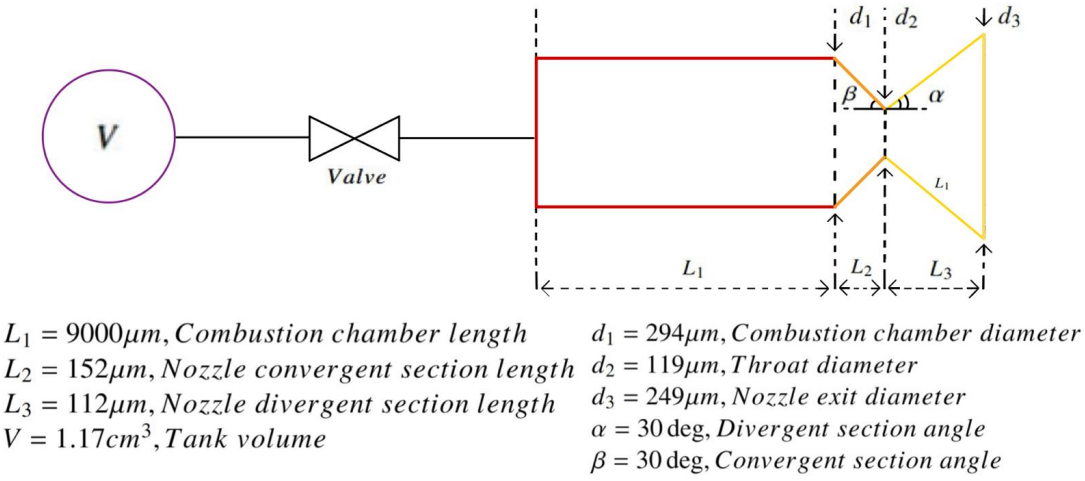

Figure 7: VLM system schematic, reporting the sizing results

3.2 Solid propellant thruster

The solid propellant model that was chosen is based on AP/HTPB/Al propellant, with 68% of Ammonium Perchlorate, the oxidizer of the mixture, 18% of Aluminum, which elevates the combustion temperature, and 14% Hydroxyl-Terminated Polybutadiene, which works both as a binder and as fuel for the thruster. This mixture ratio has a density of $\rho_{Prop} = 1762\,\mathrm{kg/m^3}$.

3.2.1 Model Assumptions

In order to simplify the analysis and focus on the fundamental performance characteristics, the following assumptions were adopted:

- Propellant grain is considered cylindrical and the combustion occurs at a constant burning area;
- Single phase flow, effects of two-phase flow aren't considered;
- The chamber walls are considered adiabatic therefore there aren't heat loss to the surroundings;
- Ignition process is not modeled and steady-state operation is assumed from the start of combustion;
- Heat conduction through the system structure is neglected;
- Expansion of the gasses through the nozzle is assumed isentropic, nozzle friction or shock losses are ignored;

- The working flow is considered as calorically perfect gas.
- The nozzle section angles (convergent and divergent) are assumed to fall within the typical range observed in comparable cases.

3.2.2 Performance study and propulsion unit sizing

To study the performance of the solid propellant micro-thruster, three values must be fixed: the pressure in the combustion chamber $P_c = 3.5\,\text{MPa}$, the combustion temperature of $T_c = 700\,\text{K}$ and the expansion ratio $\varepsilon = 20$; the values of pressure and temperature were chosen based on other studies of solid propellant MEMs [28], while the expansion ratio was fixed to obtain a nozzle efficiency of $\eta_{nozzle} = 0.4896$, computed using equation 1.

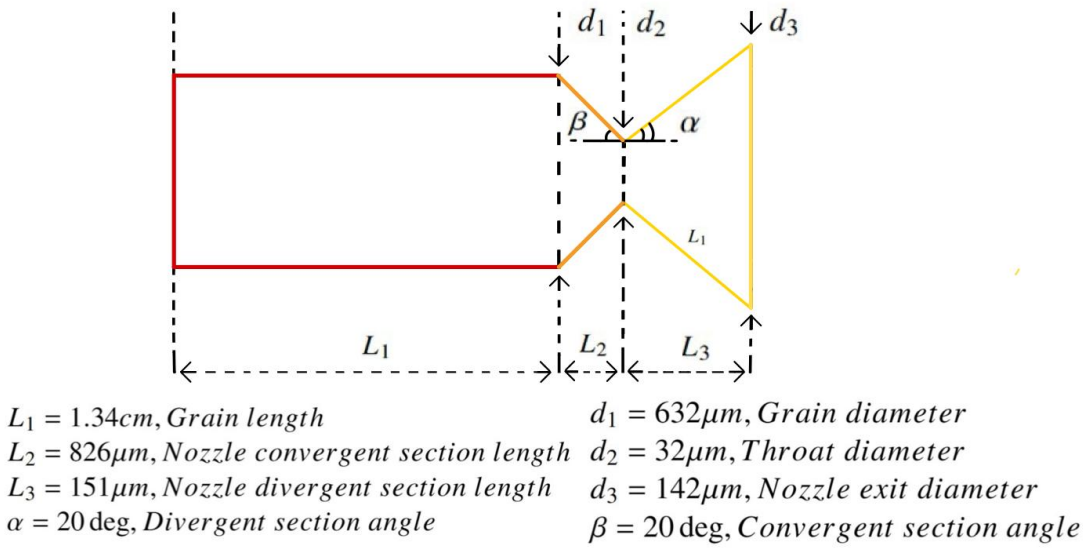

Figure 8: SPM system schematic of one thruster, reporting the sizing results

The first computations for the sizing of the propulsion unit are the same done in the section regarding the study of the VLM, the values at the exit of the nozzle are shown in table 6.

Exit temperature	Exite pressure	Exit velocity
T_e [K]	P_e [Pa]	v_e [m/s]
357.23	20913	1294.4

Table 6: Values at the exit of the nozzle for solid propellant

These values have been computed by assuming an isentropic expansion inside the nozzle so the results are all function of just the type of propellant and of the temperature and pressure in the combustion chamber.
As stated before, a fundamental parameter for the performance study is the specific impulse (equation 5), but to do so we first need to calculate the mass flow rate. The system 4 allows the computation of both the mass flow rate and throat area and the results are shown in table 7.
The two values are very low in order to balance the high exit velocity and pressure in order to obtain a nominal thrust of 5 mN, as stated in the work objectives.
From the mass flow rate, using equation 5, we compute the specific impulse: $I_{sp} = 137.01\,\text{s}$; this value is relatively high with respect to usual values for solid propellant MEMs, but this is due to not accounting for ther-

Mass flow rate	Throat area
$\dot{m}$ [mg/s]	d_t [μm]
3.7202	31.7

Table 7: Mass flow rate and throat area

mal losses and combustion inefficiencies. Thanks to this computation, we can now size the solid propellant grain.

To evaluate mass ratio MR of the spacecraft (wet mass/dry mass) it has been used the Tsiolkovsky equation:

$$MR = e^{\frac{\Delta V}{I_{sp} g_0}} \tag{12}$$

Thanks to this value and knowing the dry mass, it is possible to retrieve the propellant mass needed, simply computing $M_{prop} = M_{wet} - M_{dry} = (MR - 1)M_{dry}$, and now also the propellant volume is easy to retrieve exploiting the propellant density: $V_{grain} = 422.3451\ \text{mm}^3$

From the experimental results retrieved from previous exercise lecture [22], the mean value of the coefficients a and n are known with their relative standard deviation results. Thanks to the Vieille law, the burning rate r_b can be computed:

$$r_b = aP_c^n = 6.7\frac{mm}{s} \tag{13}$$

After that r_b is computed, there are all the data necessary to compute the burning area and the length of the grain:

$$A_b = \frac{\dot{m}}{r_b \rho_p} \quad \rightarrow \quad d_b = 633\mu m \quad \rightarrow \quad L_g = \frac{V_p}{A_b} = 1.34m \tag{14}$$

Since the burning area is really low, the resulting length of the grain is too high. In order to obtain a reasonable value of the length of the combustion chamber for each thruster, it was decided to put 100 thruster, in this way the total length can be split, obtaining a length of a single combustion chamber of $1.34cm$.

3.3 Nozzle sizing

Since the grain of solid propellant has been divided for 100 thrusters, the propulsion unit will be composed of 100 nozzles of the same dimensions. The sizing is done by using the equations 7 8 and accounting for half-angles of $\alpha = 20°$ and $\beta = 20°$; the results are in table 8.

L_{Div}	L_{Conv}	L_{Nozzle}
0.1512 mm	0.8259 mm	0.9771 mm

Table 8: Nozzle dimensions for solid propellant

3.4 Bipropellant thruster

The Bipropellant system was studied considering as oxidizer the nitrogen tetroxide (N_2O_4) and as fuel the hydrazine (N_2H_4) with a oxidizer to fuel ratio of $OF = 1.08$.

3.4.1 Model assumptions

To guide the system modeling and and component sizing is made by assuming the following hypothesis:

- Friction is neglected through the system;
- The gasses are considered calorically perfect;
- Boundaries are treated as adiabatic therefore no heat dispersion is taken into account;
- From the convergent section of the nozzle the fluid is considered isentropic;
- Two independent pressure regulators and two valves, one for each propellant line;
- The injection is modeled relying on a discharge coefficient approach;
- Flame temperature is calculated using thermodynamic equilibrium operations and the operating temperature is imposed to remain below metal limits to avoid structural degradation.
- The nozzle section angles (convergent and divergent) are assumed to fall within the typical range observed in comparable cases.

3.4.2 Sizing

Sizing begins by assuming some values that are useful for the characterization of the main thermodynamics parameters. The first step was finding the correct amount of oxidizer to fuel ratio to put in the RPA software; it was then decided to have a pressure chamber of 50 kPa in order to have a pressure high enough to avoid excessively low efficiency of the nozzle, caused by friction losses, with an expansion ratio $\epsilon = 20$ [18].
After imposing these values, we can start the computation of the main parameters in RPA and it is possible to obtain:

RPA DATA					
M_{mol} [kg/mol]	OF	γ	T_c [K]	ρ_{fuel} [kg/m^3]	ρ_{ox} [kg/m^3]
0.0184368	1.08	1.557	2760.3744	1003.7	1380

Subsequently, the pressure ratio between the nozzle exit pressure and the combustion chamber pressure ($PR = \frac{P_e}{P_c}$) is calculated using the following formula:

$$\frac{1}{\varepsilon} = \frac{A_t}{A_e} = \left(\frac{\gamma+1}{2}\right)^{1/(\gamma-1)} \left(\frac{P_e}{P_c}\right)^{1/\gamma} \sqrt{\frac{\gamma+1}{\gamma-1}\left[1-\left(\frac{P_e}{P_c}\right)^{(\gamma-1)/\gamma}\right]} \tag{15}$$

Given the analytical complexity of determining P_c directly, it was computed numerically using **Matlab®** command *fzero*, which additionally allows P_e to be derived. With this value of PR is possible to retrieve the nozzle efficiency $\eta = 49.94\%$ (Eq.1)

The results at the exit of the nozzle are reported in table 9.

Assuming a nozzle throat diameter of d_t =269 µm (fixing also the the throat area A_t) to obtain the desired thrust T=5 mN, the following formula was used to compute the area of the combustion chamber A_c:

$$A_c = \frac{A_t}{M_c}\frac{2}{\gamma+1}\left(1+\frac{\gamma-1}{2}M_c^2\right) \quad \rightarrow \quad d_c = 819\mu m \tag{16}$$

Exit temperature	Exite pressure	Exit velocity
T_e [K]	P_e [Pa]	v_e [m/s]
1382	294	3037.8

Table 9: Values at the exit of the nozzle for bipropellant

Obviously the value is really low but is compliant with the MEMS dimensions (NOTE: this results is obtained with $M_c = 0.1$ and not the usual $M_c = 0.2$).
Since the characteristic length of the combustion chamber L^* range is known from literature 10, after choosing L^* =0.76 m, by also knowing the type of bipropellant used, it is possible to compute the volume of the combustion chamber V_c:

$$V_c = L^* A_t = 43.3mm^3 \tag{17}$$

Propellants	L* [m]
Liquid F/N_2H_4	0.61 - 0.71
Liquid F/Liquid H_2	0.56 - 0.76
H_2O_2/RP-1 (with catalyst bed)	1.52 - 1.78
HNO_3/N_2H_4-based fuel	0.76 - 0.89
N_2O_4/N_2H_4-based fuel	0.76 - 0.89
Liquid O_2/NH_3	0.76 - 1.02
Liquid O_2/Liquid H_2	0.56 - 1.02
Liquid O_2/RP-1	1.02 - 1.27

Table 10: Characteristics length [15].

The value of the real combustion chamber length L_c is easy to retrieve since $L_c = V_c/A_c$. During the computation of the L_c it was found that the combustion chamber was too long (approximately 16 cm) and so it was thought that probably the mach number M_c in the combustion chamber was lower than the first hypothesis of $M_c = 0.2$.

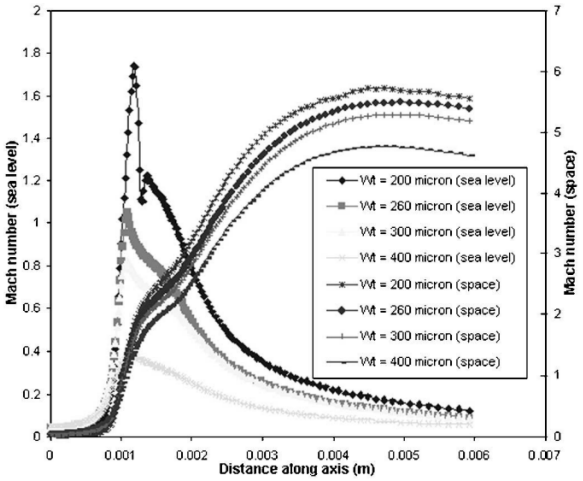

Figure 9: Mach number along the spacecraft (combustion chamber from x=0 to 1mm) [33]

So, the mach number in the combustion chamber was set to 0.1 during the computations to obtain a L_c =8.2 cm.

The mass flow rate was then computed:

$$\dot{m} = \frac{A_t \cdot p_c}{c^*} = 1.63\frac{mg}{s} \tag{18}$$

where c^* is the characteristic velocity.

The nozzle was designed by choosing arbitrarily the divergent and convergent angle that are respectively $\alpha = 30°$ and $\beta = 45°$. Doing so, the length of the nozzle computed is 1.1 mm. (7) (8)

Imposing the divergent angle α, the 2D losses λ are computed:

$$\lambda = \frac{1 + \cos(\alpha)}{2} = 0.933 \tag{19}$$

The specific impulse is computed using the formula $I_{sp} = \frac{T}{\dot{m} g_0} = 310s$ (where g_0 is the value of gravitational field at sea level); this value is high due to the low flow mass rate required to achieve the nominal thrust. Exploiting the Tsiolkovsky equation, it is possible to retrieve the mass ratio (MR=wet mass / dry mass):

$$MR = e^{\frac{DV}{I_{sp} g0}} = 1.0002 \tag{20}$$

The mass ratio is approximately equal to one and that's normal since the required DV is small, so the propellant mass is a very small percentage of the wet mass and it can be computed as in the previous sections. From the mass ratio is simple to find the propellant mass and then the oxidizer and fuel mass exploiting OF.

$$M_{fuel} = \frac{M_{prop}}{1 + OF} = 158mg \quad \rightarrow \quad M_{ox} = M_{prop} - M_{fuel} = 171mg \tag{21}$$

The mass flow rate of each fuel and oxidizer can also be computed using the formula:

$$\dot{m}_{ox} = \frac{OF}{1 + OF}\dot{m} = 0.846\frac{mg}{s} \quad \rightarrow \quad \dot{m}_{fuel} = \dot{m} - \dot{m}_{ox} = 0.783\frac{mg}{s} \tag{22}$$

The configuration of injection selected is a doublet impinging: the area of the injection of the fuel and the oxidizer are both calculated in the same way, so it follows only the example of the fuel:

$$A_{fuel} = \frac{\dot{m}}{C_d \cdot \sqrt{2\Delta P_{inj} \cdot \rho_{fuel}}} = 2.88 * 10^{-4} mm^2 \quad ; \quad A_{ox} = 2.657 * 10^{-4} mm^2 \tag{23}$$

where ΔP_{inj} is the loss in pressure due to the injection and it is dependent on the combustion chamber pressure ($15\% P_c$). Since from computation it results that the injection area is already small for both oxidizer and fuel, it was decided to have only one injector for both. So now it's easy to retrieve the diameter of the fuel and oxidizer injector.

The tank sizing process begins with determining the necessary pressure for both oxidizer and propellant tanks, by taking into consideration that the feeding system is pressure regulated with 2 valves that consumes $0.5W$ each [2], and all the losses encountered in the line are:

$$P_{tank} = P_{chamber} + \Delta P_{dyn} + \Delta P_{feed} + \Delta P_{inj} \tag{24}$$

where: ΔP_{feed} is assumed to be 0.5 atm, ΔP_{inj} is the same mentioned above and $\Delta P_{dyn} = \frac{1}{2}\rho u_p^2$ [6]

The formula (24) is general, in fact it can be applied to both oxidizer and fuel feeding lines, using the proper density ρ and velocity u_p. The calculation of $P_{oxidizer\ tank}$ and $P_{fuel\ tank}$ reveals that both values are very

similar. To streamline computations, both pressures are assumed equal to the higher of the two, specifically the oxidizer pressure of $1.150 \cdot 10^5\ Pa$.

Assuming an initial pressurizing gas temperature T_{pg} of 273 K, an initial pressurizing gas pressure P_g of 1 MPa that ensures neither the oxidizer nor the fuel reaches boiling conditions and a k_{pg} of 1.66 it is possible to compute the final temperature of the pressurizing gas after the full expansion $T_{pg,\ final}$, necessary to determine the final volume occupied by the pressurizing gas $V_{ox,\ final}$ in the oxidizer line and $V_{fuel,\ final}$ in the fuel line:

$$V_{\text{pg\_ox\_f}} = \frac{V_{\text{ox\_tank}}}{1 - \frac{P_{\text{pg\_f}}}{P_{\text{pg\_i}}} \cdot \frac{T_{\text{pg\_i}}}{T_{\text{pg\_f}}}} = 0.1734cm^3 \qquad V_{\text{pg\_fuel\_f}} = \frac{V_{\text{fuel\_tank}}}{1 - \frac{P_{\text{pg\_f}}}{P_{\text{pg\_i}}} \cdot \frac{T_{\text{pg\_i}}}{T_{\text{pg\_f}}}} = 0.2207cm^3 \tag{25}$$

From that is possible to retrieve the initial volume occupied by the pressure gas of the oxidizer and fuel:

$$V_{pg\_ox\_i} = V_{pg\_ox\_i} - V_{ox\_tank} = 0.0471cm^3 \qquad V_{pg\_fuel\_i} = V_{pg\_fuel\_i} - V_{fuel\_tank} = 0.0600cm^3 \tag{26}$$

ASSUMED DATA						
M_{dry} [kg]	α [rad]	β [rad]	M_c	ΔP_{inj} [Pa]	C_{d}	u_{p} [m/s]
2	$\pi/6$	$\pi/4$	0.1	7500	0.7	10

NOZZLE LENGHTS		
$L_{convergent}$ [mm]	$L_{divergent}$ [mm]	L_{nozzle} [mm]
0.275338	0.808872	1.084210

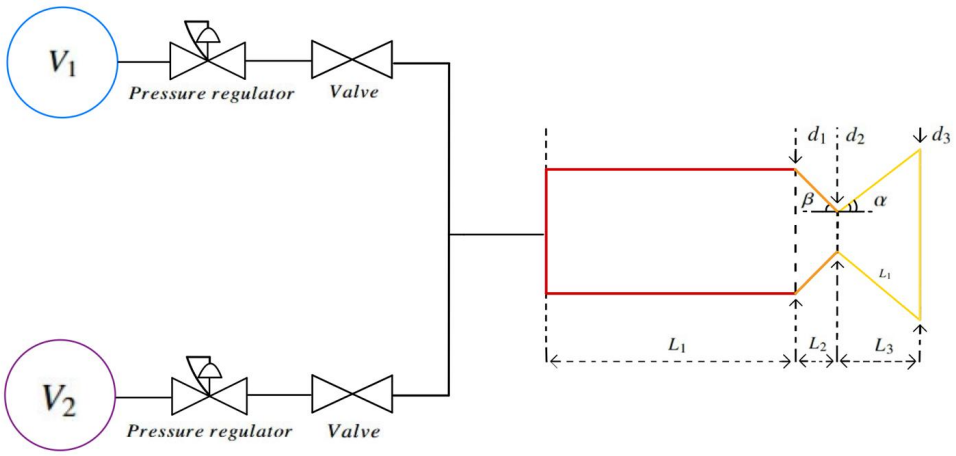

$L_1 = 8.2cm$, *Combustion chamber length*
$L_2 = 275\mu m$, *Nozzle convergent section length*
$L_3 = 809\mu m$, *Nozzle divergent section length*
$V_1 = 126mm^3$, *Oxidizer tank volume*
$V_2 = 161mm^3$, *Fuel tank volume*

$d_1 = 820\mu m$, *Combustion chamber diameter*
$d_2 = 269\mu m$, *Throat diameter*
$d_3 = 1203\mu m$, *Nozzle exit diameter*
$\alpha = 30$ deg, *Divergent section angle*
$\beta = 45$ deg, *Convergent section angle*

Figure 10: Bipropellant system schematic, reporting the sizing results

3.5 Cold gas thruster

3.5.1 Model Assumption

A cold gas thruster harnesses its energy from a pressurized propellant, without combustion or electromagnetic acceleration, making cold-gas thrusters a competitive alternative in comparison with combustion and electric based systems.

The requirements for the design are a 5 mN thrust and a $\Delta V = 0.5$ m/s, through a nitrogen-based expansion. The chosen system configuration accounts for the presence of an injector valve, a plenum which supplies constant pressure, a filter and a pressure regulator.

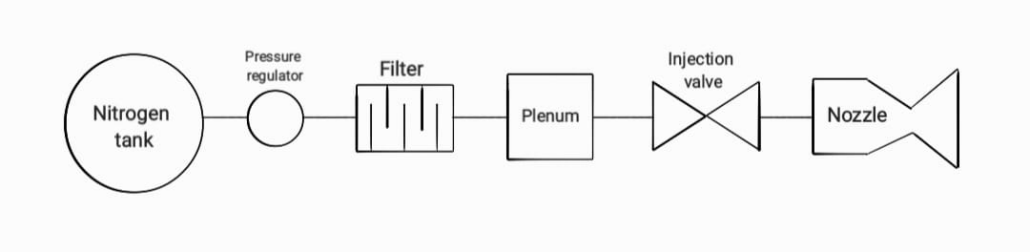

Figure 11: Preliminary hydraulic scheme for a cold gas thruster

The design accounts for the following assumptions:

- The solid boundary of the hydraulic system is smooth and therefore frictional and boundary layer effects are negligible;
- The working fluid is assumed to be gaseous and homogeneous, condensed phases might exist, but they are minimal and thus negligible.
- The gas is considered as calorically perfect.
- There is no heat transfer all over the hydraulic system and in the nozzle expansion;
- The inlet temperature is at standard conditions (25 °C);
- Microfluidics effects are neglected.
- Shock waves or flow discontinuities do not occur in the nozzle flow, and the fluid is yet isoentropic at the convergent exit;
- The flow is steady, and the transient effect is negligible;
- Chemical equilibrium is established, frozen flow assumption is considered valid;
- Nozzle is a convergent-divergent, conical and symmetric;

3.5.2 Nozzle

The pressure in the chamber has been set equal to 1.5 bar, according to recurrent values for a low-thrust cold gas thruster [11], whereas, as previously mentioned, the temperature in the chamber has been established at 25 °C. The propellant selected is gaseous nitrogen, fuel properties are provided in table 11.

Fuel	M_{mol} [g/mol]	γ	$P_{\text{sat@298 K}}$
Nitrogen	28.013	1.4	7.5 MPa

Table 11: Properties of Gaseous Nitrogen

From pre-existing literature, it was found that thrust and specific impulse grows with the increasing of the expansion ratio, eventually stabilizing as eps = 8.9 [18]. Accordingly to another references which exhibited more comparable final geometric values, a final area ratio value equal to 10 has been selected [20]. Through the application of an iterative method to the inverse of the area ratio

$$\frac{1}{\varepsilon} = \frac{A_t}{A_e} = \left(\frac{\gamma+1}{2}\right)^{1/(\gamma-1)} PR^{1/\gamma}\sqrt{\frac{\gamma+1}{\gamma-1}\left[1 - PR^{(\gamma-1)/\gamma}\right]} \tag{27}$$

the resulting pressure ratio has been found to correspond to $PR = 0.0072$, therefore, the value of the exit pressure was $P_e = 1081$ Pa . Thereafter, the throat area of the nozzle has been calculated with the following correlation:

$$C_T = \sqrt{2\frac{\gamma^2}{\gamma-1}\left(\frac{2}{\gamma+1}\right)^{\frac{\gamma+1}{\gamma-1}}} \cdot \sqrt{1 - PR^{\frac{\gamma-1}{\gamma}}} + \epsilon \cdot PR = 1.6469 \tag{28}$$

$$A_t = \frac{T}{P_c C_T} \rightarrow d_t = 160.53\ \mu\text{m} \tag{29}$$

The determination of the divergent part of the nozzle has been carried out by assuming the semi-angle of the nozzle as equal $\alpha = 20°$ [25], which is a recurrent value even in absence of the hypothesis neglecting the generation of instabilities, since a larger angle can cause rupture of the boundary layer and can result in shockwaves, extensively reducing the accuracy [20]. Thereafter, the convergent, which guides the gas towards the nozzle throat, where it reaches Mach 1, has been sized with an angle equal to $\beta = 30°$[20].
Finally, in order to complete the design specification of the nozzle, the section of the adiabatic chamber was defined, hence an assumption of the Mach number in the chamber was required. Considering that the propellant mass flux has to be accelerated through the nozzle, the value Mach = 0.2 was considered to be suitable. Since the Mach number is equal to 1 at the throat, the correlation of the expansion ratio was employed to retrieve the adiabatic chamber cross-section.

$$A_c = \frac{A_t}{M_c}\left[\frac{2}{\gamma+1}\left(1 + \frac{\gamma+1}{2}M_c^2\right)\right]^{\frac{\gamma+1}{2(\gamma-1)}} \rightarrow d_c = 276.35\ \mu\text{m} \tag{30}$$

As a consequence, the lengths relevant to the calculation of the final nozzle length are found to be

$$L_{Div} = \frac{1}{2}\frac{d_e - d_t}{tan(\alpha)} = 476.83\ \mu\text{m} \qquad L_{Conv} = \frac{1}{2}\frac{d_c - d_t}{tan(\beta)} = 100.30\ \mu\text{m} \tag{31}$$

$$\tag{32}$$

resulting in a total length of the nozzle equal to $L_{\text{noz}} = 577.14\ \mu$m. However, due the nozzle configuration, the divergence loss has to be taken into consideration. Hence, under the assumption of conical nozzle, the divergence loss factor has been computed as:

$$\lambda = \frac{1 + \cos(\alpha)}{2} = 0.9698 \tag{33}$$

A greater value of lambda could have been achieved with a lower value of α, even so the value computed was considered compliant with the requirements of the design. In order to finalize the discussion on the nozzle design, the exhaust velocity and the efficiency have been calculated as:

$$u_e = \sqrt{2\frac{\gamma}{\gamma-1}\frac{R}{M_{mol}}T_c[1-PR^{\frac{\gamma-1}{\gamma}}]} = 684.00\frac{m}{s} \tag{34}$$

$$\eta = 1 - \left(\frac{P_e}{P_c}\right)^{\frac{\gamma-1}{\gamma}} = 0.7557 \tag{35}$$

The low nozzle efficiency is attributable to the limited value of the expansion ratio, that results in a low pressure ratio. However the value obtained was considered compliant with the design assumptions.

3.5.3 Injection valve

The design process was developed based on the assumption that the ratio between the pressure drop due to the injection and the nominal chamber pressure corresponds to 16,5% [20]. First and foremost, the mass flux has been computed, and subsequently the injection valve cross section was derived by imposing a discharge parameter equal to 0.7:

$$\dot{m} = \frac{T_{\text{nominal}} - P_e A_e}{u_e \cdot \lambda} = 7.2074 \text{ mg/s} \tag{36}$$

$$A_{inj} = \frac{\dot{m}}{c_D\sqrt{2\Delta P_{inj}\rho_{Prop}}} \rightarrow d_{inj} = 212.70\ \mu\text{m} \tag{37}$$

Upon seeing that the entrance to chamber diameter and the injection valve were comparable and considering the hypothesis of absence of microfluidic effects, suitable length for the chamber was deemed equal to the diameter of the chamber itself. As a result the volume of the chamber is $V_c = 0.0166mm^2$.

3.5.4 Performance evaluation

The key parameter to estimate the performance of a propulsion system corresponds to the gravimetric specific impulse, which is computed as follows:

$$I_{sp} = \frac{T}{\dot{m}g_0} = 70.71 \text{ s} \tag{38}$$

The resulting value indicates a high level performance for a cold gas thruster propulsion system, furthermore it has been found to be consistent with pre-existing literature [11] [7].
Following the computation of the gravimetric specific impulse, it was possible to perform a mass evaluation. The mass ratio was derived through the Tsiolkovsky equation and by assuming that a dry mass of a CubeSat equal to 3kg [14]. The final value amounts to $M_p = 0.0022$ kg. Nevertheless, since the potential presence of voids in the valve could result in a catastrophic condition in case of a cold gas propulsion system owing to the low viscosity which results in an excessively high pressure, the propellant mass has been increased by 20% $M_{p+20\%} = 0.0026$ kg, in order to account for all possible leakages [4].

$$MR = \exp\left(\frac{dv}{g_0 \cdot I_{sp}}\right) \tag{39}$$

$$M_{\text{propellant}} = \text{margin} \cdot (MR - 1) \cdot M_{\text{dry}} = 0.0026kg \tag{40}$$

3.5.5 Plenum

The plenum is a defined volume which is maintained at a constant pressure, with the purpose of absorbing the potential pressure fluctuations due to the action of the injector valve and the pressure regulator. Starting from the injector valve pressure drops which have already been defined above, the pressure inside the plenum can be computed as $P_{plenum} = P_c + \Delta P_{inj} = 174.75$ kPa, whereas the volume of the plenum has been assumed as $36\,\text{mm}^3$ [12].

3.5.6 Tank sizing

From a preliminary estimation of pressure losses that took in account the injection valve, the filter, pressure regulator, the feeding line and dynamic losses, the comprehensive calculation amounted to

$$\Delta P_{tot} = \Delta P_{dyn} + \Delta P_{feed} + \Delta P_{inj} + \Delta P_{regulartor} + \Delta P_{filter} \approx 6 \div 7.5 \times 10^4 \text{ Pa} \tag{41}$$

Under these circumstances, the feeding line losses Δp_{feed} have been assumed equal to a recurrent value of 35 kPa [23], whereas dynamic losses have been computed as $\Delta p_{\text{dyn}} = \frac{1}{2}\rho u_p^2$, assuming that the velocity of the flow in the pipes corresponds to 10 m/s [23]. The necessity of defining a range stems from the fact that predicting a pressure loss coefficient for the filter and the regulator beforehand is difficult, owing to its strong dependence on system specific features.
A first evaluation of the pressure in the tank was set to coincide with the minimum value required to compensate the losses, hence the sum of those losses and the pressure in the adiabatic chamber. Following an initial sizing, the resulting volume turned out to be excessively large with respect to the overall CubeSat dimensions. In order to reduce the size, an higher value of pressure was selected from a prior literature example, where comparable values had been reported: the final value was set to 10 bar [20]. Indeed, besides exceeding the calculated minimum, it resulted in a significantly smaller dimensions, compatible with those of a 3U CubeSat. To provide an insight, by assuming a spherical geometry, the radius of the tank would be $r_{\text{tank}} = 37.98$ mm

3.5.7 Power generation

As previously mentioned, cold gas propulsive systems have a very reduced complexity, feature that makes them particularly suitable to missions with relatively simple propulsive system requirements. From a risk analysis perspective, this inherent simplicity renders them both reliable and safe, given the absence of contamination issues, due to the use of an inert and benign gas propellant. These benefits are counterbalanced by a drawback: although propellant tank and nozzle could be conveniently miniaturized according to the available system volume and mass, the valve requires a more detailed analysis. A number of publications [4], [16], [11] report that conventional valve actuation consumes a significant amount of electrical power, in the order of 1 W for holding and as high as 10 W for opening.
A potential solution to this challenge has been put forward in the publication “Design and Test of an Economical Cold Gas Propulsion System” [16], and relies on using a latching valve that requires a short electrical pulse to open and another to close. Between the pulses the thruster is magnetically latched in either the open or closed position as required, and this feature dramatically reduces power required by the thruster valves while preserving the option for small impulse bits.

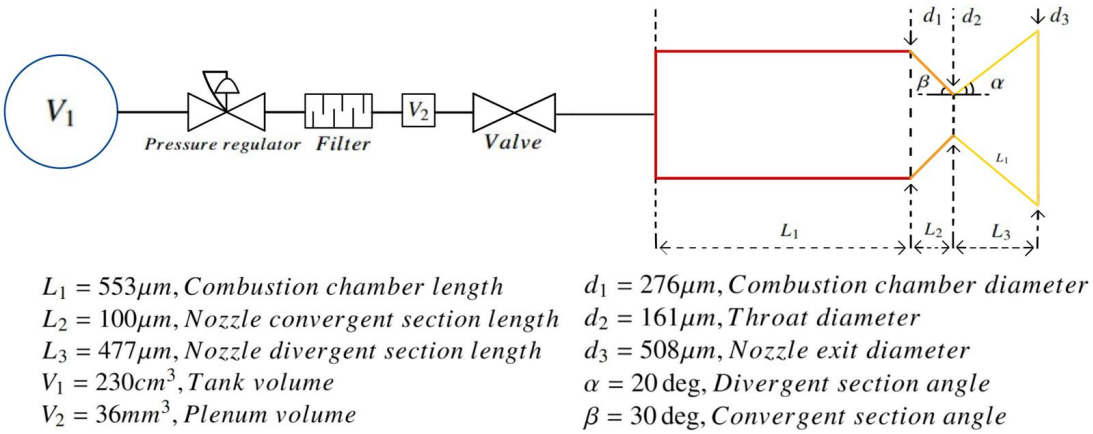

$L_1 = 553\mu m$, *Combustion chamber length*
$L_2 = 100\mu m$, *Nozzle convergent section length*
$L_3 = 477\mu m$, *Nozzle divergent section length*
$V_1 = 230cm^3$, *Tank volume*
$V_2 = 36mm^3$, *Plenum volume*
$d_1 = 276\mu m$, *Combustion chamber diameter*
$d_2 = 161\mu m$, *Throat diameter*
$d_3 = 508\mu m$, *Nozzle exit diameter*
$\alpha = 20$ deg, *Divergent section angle*
$\beta = 30$ deg, *Convergent section angle*

Figure 12: CGT system schematic, reporting the sizing results

4 Technology considerations

Given the small scales of miniaturized thruster and, as a consequence, the reduced tolerances, previous works [18] underline the necessity of high degree of fidelity techniques. The technologies which have been considered for the design of this MEMs based propulsion system are the following micro manufacturing processes:

- Micro-EDM (die-sink or wire EDM);
- Chemical etching;
- Laser-assisted-micromachining;

The previous methods present some more significant challenges if compared to those requested for the manufacture of macro-products. Among these, there are:

- the necessity of considering factors that, otherwise, can be neglected, e.g. vibrations, tool-offset, temperature
- the process of automation, due to frequent adjustments
- limitations on the materials, only ductile- and soft-materials with low-strength properties were chosen as the test materials
- tooling dimension limitations
- unwanted external forces
- dimension and performance of sensors, currently with a precision of the order of tenths of microns.

In the present scenario, the fabrication of the ceramic nozzle represents one of the main hurdles, due to its small complex structure and high hardness of the material.

Some attempts for the fabrication of a miniaturized nozzles have been done, among these ”Fabrication of ZrB_2–SiC–graphite ceramic micronozzle by micro-EDM segmented milling” [17] is taken as a reference for the design modeling of the nozzle concerned. Indeed, the aforementioned paper outlines the manufacturing process by micro-EDM technology of a micro-nozzle and in this instance the experimental results show that the machining error in the radial direction is less than 16 µm, value that has been taken as double the uncertainty related to the nozzle.

Micro-EDM refers to an EDM process performed using an electrode of micro scale geometry (5 µm to 500 µm), yielding a good surface quality (average roughness Ra down to 200 nm). In EDM, machining is performed by a sequence of electrical discharges occurring in an electrically insulated gap between a tool electrode and a workpiece where, during the discharge pulses, a high temperature plasma channel is formed, causing evaporation and melting of the workpiece itself [3].

A further significant challenge for the design is the fabrication of an injection plate and its orifice. With reference to "An Investigation into Injector Architecture for Sub-Newton Monopropellant Propulsion" [8], a Poiseuillle injector is manufactured using different methods, more specifically two methods have been selected for the injection plate concerned: chemical etching and laser-assisted micromachining.
Chemical etching is one of the oldest nontraditional machining processes. In the publication referred to above, etching has been realized with an acid etchant and geometry has been controlled by a photosensitive resistive layer, with detailing exposed onto the resist using laser light. This has been demonstrated to be the more reliable and lower cost techniques, in addition to be endowed with good repeatability and a tolerance of± 10 μm [26].
The second chosen technology is laser-assisted machining, which has gained significant interest in recent years for its potential in micro-scale processing of hard materials. The publication "Laser-assisted micromachining techniques, an overview of principles processes and applications" [13] reports a comparison between laser micromachining and other methods, emphasizing the unique advantages of laser-assisted micromachining. Some of the significant aspects are the precision in a range of 1–5 μm, the applicability across various ranges of material (e.g. glass, metals, ceramics) and the high flexibility, due to a variable pulse width.

To conclude, the analysis of production technologies enabled the study of key aspects of the design, such as sizing uncertainties, which paved the way for the use of Monte Carlo method for propagation of uncertainties.

5 Monte Carlo Analysis

5.1 Introduction

A Monte Carlo analysis is a computational technique used to model and analyze complex systems characterized by unpredictable uncertainties; it's used to estimate the probability of different outcomes when exact predictions are impossible to retrieve.

In this paper the Monte Carlo analysis was used to determine the values of the thrust, the combustion chamber pressure and the specific impulse for every propulsion system because the exact solution is impractical to obtain due to variability in different parameters caused by the difficulties of the fabrication process.
The inputs of this Monte Carlo analysis are the values calculated in the sizing sections, integrated with their respective uncertainties, taken from literature, at a level of 95% of confidence. The assumption on which the Monte Carlo is based is that all the quantities involved in this analysis come from a normal distribution, with their respective mean value μ and standard deviation σ.

After gathering all the necessary data, it was chosen to perform N^k Monte Carlo analysis, with every possible permutation of every involved parameter, where $N = 15$ (for monopropellant $N = 30$) and k is the number of quantities affected by an uncertainty (2 uncertainties for the monopropellant, 3 for all the others).
For every parameter affected by an uncertainty, it was created a Population of N random samples drawn from their respective Gaussian distribution, resulting in k vectors of size $NX1$. These vectors were then systematically combined by pairing corresponding rows, forming duplet (in case of monopropellant where $k = 2$) and triplet (in all the other cases where $k = 3$).

In order to make the method converge faster it was necessary to perform a shuffling of the douplet and triplet vectors before feeding them into the **Matlab®** code. This process randomizes the input and makes the mean

value μ and standard deviation σ graphs smoother, helping to understand when their behavior stabilizes around a stable value.
With regard to the uncertainties, as outlined in the previous chapter, the Monte Carlo method has been based on five different values. For what concerns the nozzle and the injector diameters, the fabrication technologies has been taken as a reference. Whereas for the third required value related to the power, several examples from pre-existing heater technologies have been considered, leading to a final value of 10% of the total resistance [27]. Finally, uncertainties on Vieille's law have been selected from previous designs conducted following the same methodology [22].

5.2 Reverse sizing

In order to run the Monte Carlo **Matlab®** code, a "reverse sizing" approach is used for every engine category; it consists in retrieving the performance data from the thruster geometry values obtained with the sizing.

Some difficulties have been addressed in monopropellant, bipropellant and VLM engines because there is not an assigned pressure chamber P_c at the start; this results in the impossibility to retrieve the estimated pressure loss in the injectors ΔP_{inj} (since it is assumed as a percentage of the P_c) and so, in the impossibility of the computation of the correct mass flow rate exiting the injectors.

To solve this problem, a nested loop has been implemented in the code; after giving an estimated pressure loss at the injectors as the initial input, the computation of every other necessary parameter can proceed. At the end of every iteration, a new P_c is computed, leading to a new value of ΔP_{inj}.
Iteration after iteration, eventually, the value of ΔP_{inj} stabilizes leading to a general convergence of every other parameter, such as P_c. Here is the figure that shows the convergence of the method (13)

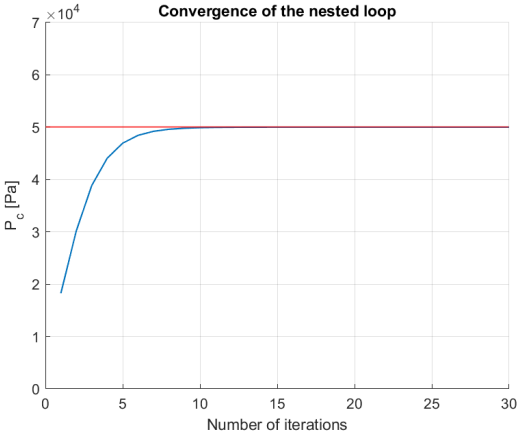

Figure 13: Bipropellant case up to 50kPa

In the VLM there was an issue during the computation of Monte Carlo because for some values, of uncertainties the chamber temperature goes below the vaporization point, which is not realistic and so these kind of data have been removed and hence the graphs of mean value and standard deviation has peaks in those points

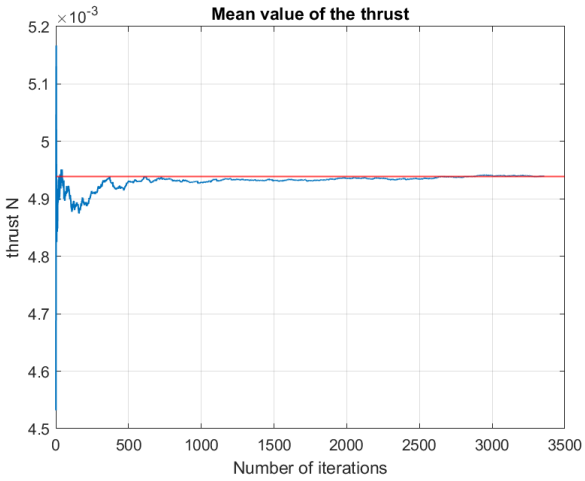

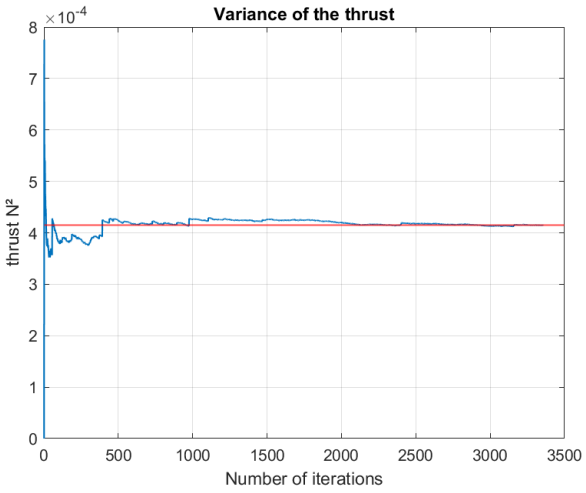

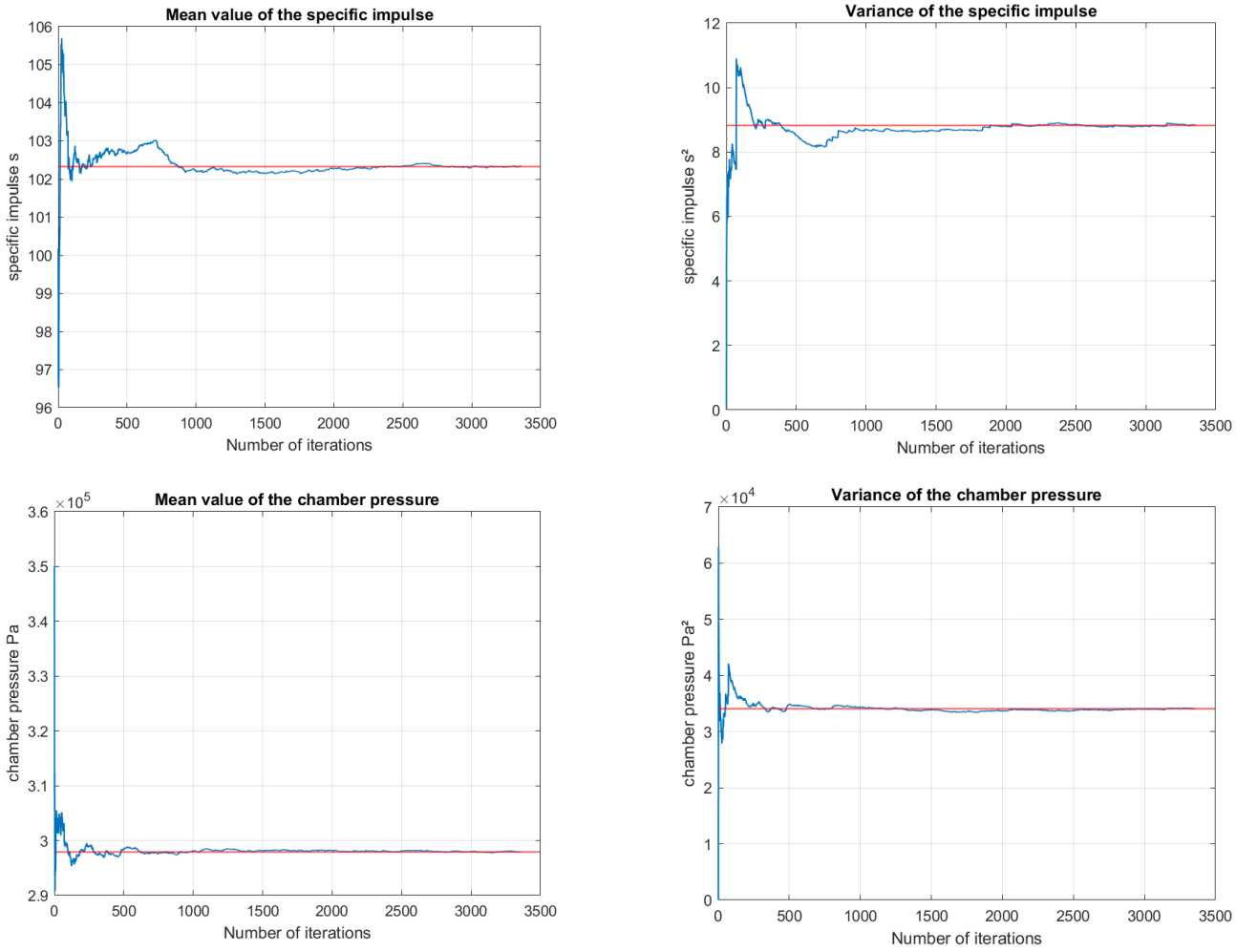

Figure 14: Monte Carlo graphs for VLM configuration

These are the mean value and variance of some parameter that comes from the VLM Monte Carlo. These graphs shows that the model converges after a certain amount of iterations.

6 Conclusions

The primary objective of the study had the main goal of analyzing in depth the world of Micro-Electro-Mechanical propulsion systems through a detailed analysis of the current configurations in development and by focusing on the performances of a 3U-CubeSat with a $T = 5\,\text{mN}$ for each thruster in the configuration and a total mission $\Delta v = 0.5\,\text{m/s}$. For each of the proposed models (Solid Propellant, Vapor Expansion, Bipropellant and Cold Gas) the typical values of interest have been computed, but it is crucial to keep in account that these computations were based on multiple simplifying assumptions (some of the recurring one: adiabatic walls, isentropic flow in the nozzle, no heat dispersion, no friction), so the results could show significant differences with respect to the performances of real MEMs. The final results are listed in table 12 and 13. From tables it is noticeable that all the value of thrust and DV fall into the range of the required value and this is also a hint that the Monte Carlo model has been computed correctly.

Final outcomes with uncertainties				
	T $[mN]$	I_{sp} $[s]$	DV $[m/s]$	Nozzle efficiency η $[-]$
Vapor expansion	4.892 ± 0.751	100.01 ± 15.82	0.486 ± 0.077	0.571 ± 0.035
Solid propellant	5.060 ± 0.521	138.55 ± 3.78	0.504 ± 0.009	0.492 ± 0.089
Bipropellant	5.013 ± 0.909	309.46 ± 2.61	0.499 ± 0.004	0.499 ± 0.013
Cold gas	5.198 ± 1.447	70.93 ± 0.78	0.499 ± 0.003	0.754 ± 0.014

Table 12: Final results of the report for values with uncertainties

Final outcomes				
	W $[W]$	V_c $[mm^3]$	V_{tank} $[cm^3]$	L_{nozzle} $[mm]$
Vapor expansion	13.4220 ± 1.3422	0.6123	1.1690	0.2635
Solid propellant	–	4.2235	0.4223	0.9771
Bipropellant	1	43.3	0.287	1.0842
Cold gas	[1 – 10]	0.0166	229.56	0.5771

Table 13: Other results of the report

6.1 Comparative analysis and Final considerations

Upon completing a detailed analysis of four different MEMS-based propulsion systems for CubeSat applications, by means of a series of assumptions and simplified model approach, four different designs have been delineated. The aforementioned configurations come with different performance parameters and each one provides a trade-off between several characteristics. The main criteria taken in consideration to establish whether a technology was deemed more effective than the other were the power consumption, the specific impulse, the volume occupied by the system, the feasibility from a technical point of view and the fulfillment of the requirements.

The Vaporizing Liquid Micro-thrusters main advantages with respect to the other configurations are the very low tank and chamber volumes that allow the VLM to be easily stored in any 3U-CubeSat while ensuring a good specific impulse. On the other hand, the main drawback is represented by the very high power consumption, which is often too high for the satellites taken into consideration; one solution for this problem could be developing satellites with more solar arrays, in order to upgrade the power generation system. As stated before, the comparison with a real prototype gave similar performance results and this gives credibility to the values obtained through sizing.

Since the solid propellant MEMs work by igniting a grain composed by a mixture of fuel and oxidizer, all the power consumption goes into the igniter, but, since one of the assumption made in this study was to not account for it, the total power consumption is considered zero, so no comment on this value can be done in this report. It's also important to note that the volume of the chamber refers to a single thruster, while the volume of the propellant considers all 100 grains. The specific impulse is better than the one of the cold gas and vapor expansion thruster, highlining the fact that this kind of propulsion system is more focused on power than accuracy.

The bipropellant is a competitive solution since thrust can be moduled with different burn (a thing that the

solid can't do) and also can keep an higher specific impulse in comparison with the other engine configuration examined in this report. Although, to obtain these kind of performances, it is required an high temperature in the combustion chamber and also in the nozzle (since T_e is higher than 1300k). This can cause some problem in the temperature range that the material of this kind of engine has to withstand. In addition, the specific impulse has to be checked in a better way considering the small size of a the combustion chamber and so the assumption of friction should be take into account.

From the point of view of feasibility, cold gas represents the simplest and more reliable technology. A notable advantage of cold thrust is unequivocally represented by the high grade of simplicity and reliability of the system. However, the performed analysis has highlighted some fundamental drawbacks: primary, the limited specific impulse, which denotes the minimum value among the other configurations. This aspect can be justified by the absence of combustion, considering that the system relies exclusively on the expansion of a pressurized gas through a nozzle. Secondly, the thrust value reported in table shows remarkably high uncertainty. Before any justification is proposed, a further specification is required: the micro-nozzle geometry, especially throat and expansion ratios, plays a critical role in performance, and even small changes significantly impact thrust and efficiency due to scaling effects. Therefore, this deviation could be due to the adoption of an alternative manufacturing process for this system, which, unlike the others, is associated with a different uncertainty level. Finally, as evidenced in the previous chapter, power required represents a pivotal aspect, in particular, the valve is a critical component that could be further optimized with suitable investigations.

To conclude the comparative analysis, the solid propellant constitutes an effective solution in the case in which only a single firing is required being a "one-shot" propulsive system. Another significant optimizable feature that can be taken in account is the reliability of the overall configuration, for which the cold gas thruster represents an effective solution, despite low performances, being the most reliable among the options. Finally, vapor liquid expansion represents a viable option due to the use of water, which represents a safer alternative to handle. Hence, in an overall trade-off, the last kind of propulsion system could be favored, despite having lower performance parameters compared to bipropellant and solid propulsion systems.

In future studies, a more detailed analysis could be conducted considering less exemplifying hypotheses, since aspects such as microfluidodynamics have been completely overlooked, and this choice could have significantly influenced the performance. A second suggestion originates from the evaluation of the manufacturing technologies, indeed, through a comparison, it was observed that the use of lasers provides a notable advantage. The cold gas serves as a representative example, since a different technological solution was adopted with respect to the others. However, laser technology is still in the early stages of development, and further advancements are needed to fully leverage its potential. A third aspect worth discussing is the criticality of miniaturization, thus far the research has been primary centered on nozzle, there is aplenty of literature example for micro nozzle, whereas references on miniaturization of valves remains limited, highlighting the need for more focused studies in this area. The constraints imposed by current technologies also limit the choice of materials, emphasizing the importance of further investigation on the use of alternative material feasibility. Finally, in-depth research would be required on the dimensioning of the micro combustion chamber, which must withstand significant stresses, since with a traditional modeling in terms of typical Mach number values result in excessively long chambers.
In light of the analysis conducted, all the aforementioned considerations suggest that a combination of less exemplifying hypothesis, an optimization of production technologies and a further research on miniaturization, could lead to significant improvements in performance.

7 Autorship Declaration

Member Name	Technical Tasks
Matteo Maria Basci	Configuration skematics, Solid propellant model
Emanuele Bianco	Bipropellant model, Monte Carlo analysis
Filippo Chini	VLM model, Solid propellant model
Antonio De Gennaro	Cold gas model, Micro-Nozzle Efficiency
Federico Ferrara	Cold gas model and literature, uncertainty and technology literature
Chiara Alessia Guffanti	Cold gas model and literature, uncertainty and technology literature
Mantas Kazėnas	Micro-nozzle efficiency, literature analysis
Luca Matteotti	VLM model, literature analysis
Riccardo Mazzitti	Bipropellant model, Monte Carlo analysis

References

[1] Abdulla Alnajim. "Numerical study of MEMS-Based vaporizing liquid microthruster for CubeSats". PhD thesis. University of Sheffield, 2021.

[2] J Bejhed et al. "Advanced flow control devices based on MEMS technology for electric propulsion". In: *33th International Electric Propulsion Conference, Uppsala, Sweden*. 2013.

[3] Samuel Bigot, Giuliano Bissacco, and Joško Valentinčič. "Die-sinking Micro EDM for Complex 3D Structuring". In: 2011.

[4] K. Cheah et al. "Cold gas microthruster". In: *Space Micropropulsion for Nanosatellites: Progress, Challenges and Future*. Elsevier, 2022, pp. 23–50.

[5] Maria Grazia De Giorgi et al. "Preliminary results concerning the development of a water-propellant vaporizing liquid microthruster for small satellites". In: *8TH EUROPEAN CONFERENCE FOR AERONAUTICS AND SPACE SCIENCES (EUCASS)*. EUCASS association. 2019.

[6] Stefano Dossi. "Exercise session". In: *Polimi* (2025).

[7] Terry Stevenson E. Glenn Lightsey and Matthew Sorgenfrei. "Development and Testing of a 3-D-Printed Cold Gas Thruster for an Interplanetary CubeSat". In: (2018).

[8] Ewan Alexander Patrick Fonda-Marsland et al. "An Investigation into Injector Architecture for Sub-Newton Monopropellant Propulsion". In: *8th European Conference for Aeronautics and Space Sciences : (EUCASS)*. 2019. URL: https://eprints.soton.ac.uk/448543/.

[9] Donato Fontanarosa et al. "Fabrication and embedded sensors characterization of a micromachined water-propellant vaporizing liquid microthruster". In: *Applied Thermal Engineering* 188 (2021), p. 116625.

[10] Donato Fontanarosa et al. "Flow regime characterization of a silicon-based vaporizing liquid microthruster". In: *Acta Astronautica* 193 (2022), pp. 691–703.

[11] Moog Inc. *Cold Gas Thrusters Datasheet*. 2022. URL: https://www.moog.com/content/dam/moog/literature/sdg/space/propulsion/moog-coldgasthrusters-datasheet.pdf.

[12] S. Janson, H. Helvajian, and K. Breuer. "MEMS, microengineering and aerospace systems". In: *30th Fluid Dynamics Conference*. DOI: 10.2514/6.1999-3802. URL: https://arc.aiaa.org/doi/abs/10.2514/6.1999-3802.

[13] Md Omar Al Javed and Adib Bin Rashid. "Laser-assisted micromachining techniques: an overview of principles, processes, and applications". In: *Advances in Materials and Processing Technologies* (2024), pp. 1–44. DOI: 10.1080/2374068X.2024.2397156. URL: https://doi.org/10.1080/2374068X.2024.2397156.

[14] Eberhard Gill Jian Guo Jasper Bouwmeester. *From single to formation Flying CubeSats: an update of the delfi Programme*.

[15] Sungkwon Jo et al. "Performance Evaluation on Characteristic Length Variation of H_2O_2/Kerosene Bipropellant Rocket Engine". In: 2011. URL: https://api.semanticscholar.org/CorpusID:108272178.

[16] Jesus ACOSTA Joseph M. Cardin. "Design and Test of an Economical Cold Gas Propulsion System". In: (1999).

[17] Huichao Li et al. "Fabrication of ZrB2–SiC–graphite ceramic micro-nozzle by micro-EDM segmented milling". In: *Journal of Micromechanics and Microengineering* 28.10 (2018). DOI: 10.1088/1361-6439/aad79b. URL: https://dx.doi.org/10.1088/1361-6439/aad79b.

[18] Xinjie Li et al. "Influences of geometry configurations on the performance of micro-nozzles". In: *Acta Astronautica* 215 (2024), pp. 618–630.

[19] Xuhui Liu et al. “Design, fabrication and test of a solid propellant microthruster array by conventional precision machining”. In: *Sensors and Actuators A: Physical* 236 (2015), pp. 214–227.

[20] M.C. Louwerse. “Cold Gas Micro Propulsion”. English. PhD Thesis - Research UT, graduation UT. Netherlands: University of Twente, 2009. ISBN: 978-90-365-2903-7.

[21] Luigi T. De Luca. “Energetic Problems in Aerospace Propulsion Notes for Students Chapter 03 Gas-dynamics of Thrust Nozzles”. In: *SPLab, Department of Aerospace Engineering, Politecnico di Milano* (2025).

[22] Filippo Maggi. “Baria motor flipped class for the study of the Vieil law”. In: *Polimi* (2025).

[23] Professor Maggi. *Space Propulsion lecture slides ”LRM”*.

[24] Juergen Mueller et al. “Design, analysis and fabrication of a vaporizing liquid micro-thruster”. In: *33rd Joint Propulsion Conference and Exhibit*. 1997, p. 3054.

[25] Juergen Mueller et al. “Design, analysis and fabrication of a vaporizing liquid micro-thruster”. In: *33rd Joint Propulsion Conference and Exhibit*. DOI: 10.2514/6.1997-3054. eprint: https://arc.aiaa.org/doi/pdf/10.2514/6.1997-3054. URL: https://arc.aiaa.org/doi/abs/10.2514/6.1997-3054.

[26] P Nageswara Rao and Deepak Kunzru. “Fabrication of microchannels on stainless steel by wet chemical etching”. In: *Journal of Micromechanics and Microengineering* 17.12 (2007), N99. URL: https://dx.doi.org/10.1088/0960-1317/17/12/N01.

[27] Omega. *Mica insulated strip heaters - Datasheet*.

[28] EA Parra, KJS Pister, and C Fernandez-Pello. “Solid-propellant micro-thruster”. In: *The Sixth International Workshop On Micro and Nanotechnology for Power Generation and Energy Conversion Applications, Nov*.

[29] Marsil AC Silva et al. “A comprehensive model for control of vaporizing liquid microthrusters”. In: *IEEE Transactions on Control Systems Technology* 27.6 (2018), pp. 2606–2613.

[30] Marsil AC Silva et al. “A review of MEMS micropropulsion technologies for CubeSats and PocketQubes”. In: *Acta Astronautica* 143 (2018), pp. 234–243.

[31] TX Van Wees. “Characterization and testing of a mems vaporizing liquid microthruster for small satellite propulsion”. PhD thesis. Master’s thesis, TU Delft, 2017.

[32] Logan T Williams, Michael McDonald, and Michael Osborn. “Performance characterization of a low Reynolds number micro-nozzle flo”. In: *51st AIAA/SAE/ASEE Joint Propulsion Conference*. 2015, p. 3924.

[33] Kaili Zhang, S.K. Chou, and S.S. Ang. “MEMS-based solid propellant microthruster design, simulation, fabrication, and testing”. In: *Journal of Microelectromechanical Systems* 13.2 (2004), pp. 165–175. DOI: 10.1109/JMEMS.2004.825309.